International Journal of Computational Methods and Experimental Measurements
https://www.acadlore.com/journals/IJCMEM

Validated Numerical Model of a Lightweight Trickle-Flow Solar Water Heater for Tropical Applications

Nugroho Agung Pambudi*, Dony Marly Martiawan Siregar, Desita Kamila Ulfa, Danny Rizki Sofyan Permana Putra

Department of Mechanical Engineering Education, Universitas Sebelas Maret, 57126 Surakarta, Indonesia

* Correspondence: Nugroho Agung Pambudi (agung.pambudi@staff.uns.ac.id)

Received: 10-28-2025 **Revised:** 12-09-2025 **Accepted:** 12-24-2025

Citation: N. A. Pambudi, D. M. M. Siregar, D. K. Ulfa, and D. R. S. P. Putra, "Validated numerical model of a lightweight trickle-flow solar water heater for tropical applications," *Int. J. Comput. Methods Exp. Meas.*, vol. 13, no. 4, pp. 882–895, 2025. https://doi.org/10.56578/ijcmem130410.

Abstract: The increasing global energy crisis and concerns about environmental impacts are driving the development of efficient and low-cost renewable energy systems. Solar water heaters (SWH) are an alternative, specifically in tropical countries such as Indonesia, which receive solar radiation intensity of 4–6 kWh/m^2/day. Therefore, this study aimed to model the thermal performance of trickle-flow SWH using a lightweight composite material called polymethyl methacrylate (PMMA) as cover and galvalume for the heat absorber plate, which has previously been validated through experiments. The simulation model was developed using a transient lumped-parameter energy balance method and was implemented in Python with minute-by-minute interpolated meteorological data. Model validation was conducted by comparing simulated and experimental inlet and outlet temperatures. It reproduced the main temperature trends and peak values observed in the experiments. Statistical evaluation further indicated a high level of accuracy, with root-mean-square error (RMSE) values of up to 0.81°C and a coefficient of determination (R^2) of 0.986 for outlet temperature. Additional parametric analyses showed the effects of flow rate and tank volume on thermal efficiency. These effects were visualized using efficiency contour plots, while confidence bands were applied to present simulation uncertainty. In general, the results confirmed the feasibility of using lightweight materials in solar collectors and showed the capability of numerical-statistical models for performance prediction as well as design optimization. These findings supported the development of efficient and low-cost SWH systems for tropical regions.

Keywords: Solar water heaters; Trickle-flow; Thermal modeling; Lightweight materials; Root-mean-square error; Statistical validation

1 Introduction

The global energy crisis, largely driven by continued dependence on fossil fuels, has intensified the search for clean, efficient, and sustainable alternative energy solutions [1, 2]. Among the available renewable options, solar energy holds a strategic position, particularly in tropical countries such as Indonesia, which receive a high level of solar radiation intensity throughout the year [3–5]. Having an average solar radiation potential of 4–6 kWh/m^2/day, the country has substantial opportunities to deploy solar energy technologies, especially solar water heaters (SWH), for both domestic and commercial applications [6].

SWH represents a practically relevant application of solar energy because of the simple construction, low operational costs, and ability to directly replace fossil-based energy for water heating [7, 8]. In this context, an economically attractive configuration is the open flow (trickle flow) system, which uses a heat absorber plate and a lightweight, transparent cover. Materials such as galvalume for the absorber and polymethyl methacrylate (PMMA) for the cover provide advantages in terms of low weight, ease of fabrication, and reduced production costs when compared with conventional metals such as copper or aluminum [9–11].

Previous studies showed that the thermal performance of SWH systems was strongly influenced by collector orientation, system configuration, and the material used [12–14]. An experimental investigation of a trickle-flow SWH equipped with a lightweight PMMA–galvalume configuration evaluated four collector orientations, namely east, east +30°, south, and north. The results signified that the east-facing orientation achieved the highest thermal

efficiency, reaching 32.7%, and produced a maximum outlet water temperature of 45.8℃. These outcomes showed that, in tropical climates, SWH performance could be substantially improved through appropriate orientation selection combined with the use of lightweight materials.

The predictability and generalizability of purely experimental results are limited, particularly when a wide range of system parameters should be explored. Therefore, numerical methods based on mathematical simulation are essential for conducting broader and more efficient analyses [15, 16]. This study focuses on the development of a transient numerical model to simulate the thermal behavior of a lightweight trickle-flow SWH, which is validated using experimental data. The model is implemented in Python as a numerical computation platform. By incorporating microclimate variables, including global solar radiation (G_T), ambient air temperature (T_a), and wind speed (V_a), the model represents the transient temperature dynamics of the SWH system. These meteorological inputs are interpolated on a minute-by-minute basis to enable accurate prediction of both inlet and outlet fluid temperatures [17, 18].

Model validation is conducted through a direct comparison between simulated and experimental data, with particular priority on the east orientation, which has been identified as optimal. Model accuracy is evaluated using statistical indicators, including the Mean Absolute Error (MAE), Mean Bias Error (MBE), and the coefficient of determination (R^2). These metrics quantify the magnitude of the absolute error, the presence of systematic bias, and the degree of agreement between the model predictions and the measured data, respectively [19]. Following the discussion, the results signify that the model reproduces the experimental temperature trends with high accuracy, producing an MAE of 0.81℃ and an R^2 value of 0.986 for the outlet temperature.

Most existing studies on SWH system modeling focused on closed systems using selective coatings in a flat plate collector (FPC) configuration. The importance of selecting collector orientation based on user consumption patterns was explained by Khanghahi et al. [20]. Yunianto reported an efficiency increase of up to 40.55% when the collector was oriented at east +30° and equipped with a single pane of glass [21]. Consequently, numerical models for open SWH systems with trickle flow configuration constructed from lightweight materials and applied in tropical regions remained scarce. Relating to the discussion, only a limited number of studies had addressed their development and validation.

This study addresses the identified gap through three principal contributions. First, the analysis develops a thermal numerical model for a trickle-flow-based SWH system constructed using lightweight materials, which is validated against experimental data. Second, the accuracy of the proposed model is evaluated using comprehensive statistical indicators, namely, RMSE, MAE, MBE, and R^2. Third, this study assesses the applicability of the model as a tool for supporting the design and optimization of efficient and affordable SWH systems, respectively. In addition, the proposed framework provides a basis for extending the analysis to other operational parameters, such as variations in flow rate, tank capacity, and alternative absorber materials.

2 Methods

2.1 Study Design

This study built upon a previous experimental investigation that evaluated the performance of a trickle-flow solar collector using galvalume as the absorber plate and PMMA as the transparent cover.In that study, the water inlet (T_{in}) and outlet (T_{out}) temperature data were recorded every 30 minutes between 9:00 a.m. and 3:00 p.m. Simultaneously, meteorological data, including G_T, T_a, and V_a were collected to support the analysis.

The follow-up study focused on developing a Python-based numerical model to simulate the thermal response of the system per minute. The use of Python served solely as a computational platform for data management, time stepping, and visualization. This did not affect the physical formulation or validation of the model. The model incorporated dynamic collector efficiency formulas, flow corrections, and heat-loss calculations for both the collector and the storage tank. In addition, Major input parameters included the heat transfer coefficient, fluid mass, and specific heat capacity. Simulation results were directly compared with experimental measurements to evaluate model accuracy and explain potential deviations arising from environmental factors or measurement errors.

2.2 Collector Design and Fabrication

The SWH system design used in this analysis is shown in Figure 1. The main collector consisted of a corrugated galvanized sheet that functioned as the absorber plate and was covered with a transparent PMMA layer to improve the greenhouse effect and reduce convective heat loss. Subgraph (a) of Figure 1 shows the overall system design, including a water storage tank, a circulation pump, a support frame, and a corrugated collector. The entire system was installed at a tilted angle corresponding to the optimal orientation for solar radiation absorption, as shown in Table 1.

Subgraph (b) of Figure 1 shows the fluid flow scheme and the locations of the thermocouple sensors installed at the inlet, outlet, and center of the collector for temperature measurement. Meanwhile, Subgraph (c) of Figure 1 shows

the fabricated and field-tested SWH system prototype. Insulation material, consisting of multiplex panels coated with aluminum foil, was installed at the bottom to minimize conductive heat loss to the surrounding environment.

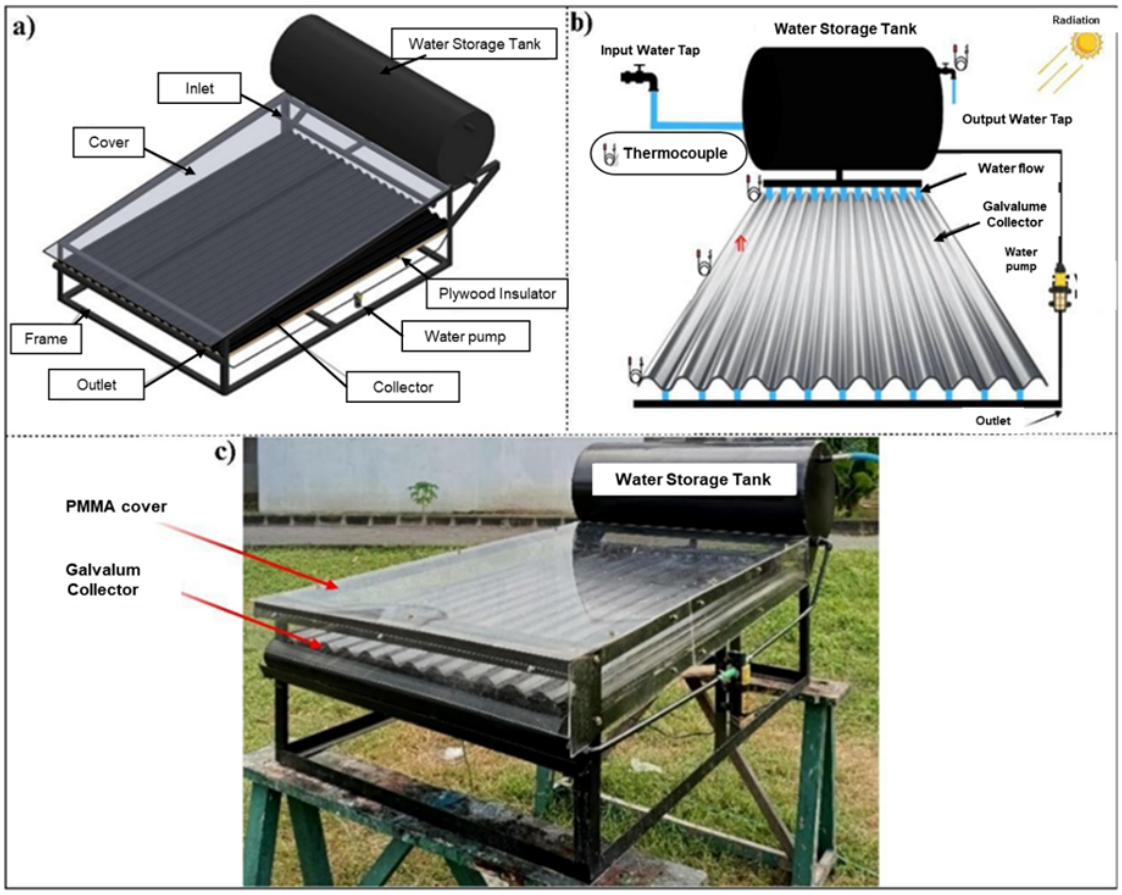

Figure 1. Solar water heaters (SWH) system design

Table 1. SWH system design specifications

Specifications	Values	Notes
Collector type	Open trickle flow	Gravity drip water
Absorber plate	Corrugated galvalume: 0.25 m × 1.5 m × 1 mm	Effective area: 1.65 m^2
Top cover	Polymethyl methacrylate: 2 mm ($\tau \approx 0.85$)	Air gap: 30 mm
Frame	Meranti wood + varnish coating	Inclination angle: 15°
Flow system	DC pump: 12 V, 3 L/min	Measured flow rate: 0.00005 m^3/s
Tank	Cylinder: 130 L, $\oslash \approx 0.454$ m, h = 0.8 m	Surface area: 1.46 m^2

2.3 Measurement Instruments

Table 2. Measurement instrument specifications and parameters used in the study

Parameters	Sensors	Accuracy	Recording Interval
Global solar radiation (G_T)	SP-Lite2 Pyranometer	± 5 W/m^2	30 minutes
Ambient air temperature (T_a)	Type-K Thermocouple	± 0.5℃	30 minutes
Wind speed (V_a)	Cup Anemometer	± 0.1 m/s	30 minutes
T_{in} & T_{out}	Type-K Thermocouple	± 0.3℃	30 minutes
Tank temperature (T_t)	PT-100	± 0.2℃	30 minutes
Water flow rate	Rotameter	± 0.05 L/min	60 minutes

The measurement instruments used in this study comprised devices designed to periodically record the primary parameters of the solar collector system, as shown in Table 2. Inlet and outlet water temperatures were measured using high-accuracy digital K-type thermometers, while G_T was recorded through a calibrated pyranometer. T_a was measured using a digital thermo-hygrometer, and V_a was recorded through a digital anemometer. All measurements were collected at 30-minute intervals from 9:00 a.m. to 3:00 p.m., yielding a total of 13 data points, which captured variations in thermal and environmental conditions over the operating time of the collector.

2.4 Numerical Model

This study developed a numerical model to simulate the thermal performance of a galvalume-collector-based SWH system. The simulations were implemented in Python due to its flexibility in data processing, visualization, and integration with thermodynamic equations. During the process, the model was formulated using a discrete-time per-minute method to correspond with the temporal resolution of the experimental observations.

2.4.1 Basic assumptions

Several assumptions were adopted during the analysis to simplify the numerical calculations. The water flow was assumed to be steady at each minute, with a Reynolds number (R_e) below 2000, justifying the use of a laminar flow regime. Heat conduction in the galvalume absorber plate was considered one-dimensional due to its very small thickness. In addition, radiative heat losses to the sky and the ambient environment were combined into a single overall heat-loss coefficient (U_L). Water in the storage tank was assumed to be perfectly mixed, leading to a uniform tank temperature at each time step. Additionally, the heat capacity of the absorber plate was neglected to improve computational efficiency, and this assumption was examined further in the sensitivity analysis. Relating to these assumptions, the Python-based model generated temperature predictions that were subsequently validated against experimental data.

2.4.2 Basic collector energy equation

In the SWH system, collector efficiency was strongly influenced by the temperature difference between the fluid and the environment as well as by the intensity of solar radiation. During the process, the energy absorbed by the collector was calculated as the difference between the incoming solar radiation energy and the heat losses to the environment.

•Collector total heat loss coefficient:

$$U_L = U_0 + U_1 \times V_a \tag{1}$$

where, U_L was the total heat loss coefficient of the collector (W m^{-2} K^{-1}), which consisted of U_0, representing heat loss due to free convection (W/m^2·K). It also comprised $U_1 \times V_a$, which signified forced convective heat loss induced by V_a. The coefficient U_1 was a constant that characterized the influence of V_a on convective heat transfer (W m^{-2} K s m^{-1}). In addition, the variable V_a was the wind speed at the collector surface (m/s). As V_a increased, the value of U_L increased, showing a greater heat loss to the surrounding environment.

•Dynamic collector efficiency:

$$\eta_c = \eta_0 - a_1 \times \frac{T_f - T_a}{G_T} \tag{2}$$

where, η_c was the actual collector efficiency, while η_0 represented the efficiency under ideal conditions with no heat loss. The parameter a_1 signified the efficiency degradation constant (m^2 K W^{-1}), and T_f was the fluid temperature in the collector (℃). Additionally, T_a represented the ambient air temperature (℃), and G_T signified the total solar radiation intensity (W/m^2).

•Effective radiation entering the collector (optical correction):

$$G_{T,eff} = \alpha \times \tau \times G_T \tag{3}$$

where, $G_{T,eff}$ was the effective radiation absorbed by the collector surface (W/m^2), and α represented the absorptivity. The variable τ was the transmittance of the glass plate, and G_T signified the total solar radiation intensity (W/m^2).

•Heat energy absorbed by the collector:

$$Q_S = F_r \times A_c \times \eta_c \times G_{T,eff} \tag{4}$$

where, Q_S was the heat energy absorbed by the collector (W), while F_r represented the collector efficiency factor in Eq. (4). The variable A_c was the collector surface area (m^2), and η_c signified the collector efficiency. In addition, $G_{T,eff}$ was the effective radiation entering the collector (W/m^2).

•Heat loss from the collector to the environment:

$$Q_L = U_L \times A_c \times (T_m - T_a) \tag{5}$$

where, Q_L represented the heat energy lost to the environment (W), while U_L signified the total heat loss coefficient (W m^{-2} K). The parameter A_c was the collector area (m^2), T_m represented the average fluid temperature in the collector (℃), and T_a was the ambient air temperature (℃).

•Net energy acquired by water:

$$Q_N = Q_S - Q_L \tag{6}$$

where, Q_N was the net energy received by water (W) in Eq. (6). In addition, Q_S signified the absorbed heat energy, and Q_L was the lost heat energy.

•Water temperature increased due to net energy:

$$\Delta T = \frac{Q_N}{\dot{m} \times C_p} \tag{7}$$

where, ΔT was the water temperature increase (℃), while Q_N represented the net energy (W). The variable $\dot{m}$ was the water mass flow rate (kg/s), and C_p signified water specific heat capacity (J kg^{-1} K).

•Fluid temperature difference:

$$\Delta T = T_{\text{out}} - T_{\text{in}} \tag{8}$$

where, ΔT represented the fluid temperature increase (℃), where T_{out} was the fluid temperature at the collector outlet, and T_{in} was the fluid temperature entering the collector. This temperature difference quantified the amount of heat energy effectively transferred to the fluid during the heat absorption process in the collector.

2.4.3 Flow factor correction

The flow factor (F_r) represented the efficiency of energy absorption by the collector, based on the fluid flow rate and its heat transfer characteristics. The value of F_r was not constant and required correction to account for actual operating conditions, such as variations in mass flow rate and heat loss. In this simulation, F_r was calculated using an analytical method based on the heat transfer theory of Duffie & Beckman, and was capped at a maximum of 0.85 to maintain consistency with experimental performance. Correcting F_r was crucial, as this value directly determined the amount of energy absorbed by the collector and transferred to the fluid.

$$F_r = \frac{\dot{m}C_p}{A_c U_L}\left(1 - e^{-\frac{A_c U_L}{\dot{m}C_p}}\right) \tag{9}$$

where, F_r was the collector efficiency factor, $\dot{m}$ represented the fluid mass flow rate (kg/s), and C_p signified the fluid specific heat capacity of the fluid (J kg $^{-1}$ K). A_c corresponded to the collector surface area (m^2), while U_L represented the collector heat loss coefficient (W m^{-2} K). The parameter e was the Euler number used in the exponential function to describe the spatial distribution of heat losses in the collector.

2.4.4 Tank mixing and heat loss

The mixing process in the storage tank was assumed to be perfect, signifying that the water temperature in the tank was uniform at each time step due to mixing induced by the inlet flow. The model used a mass-and-energy balance method to calculate the updated average tank temperature, considering both the inlet water temperature (T_{out}) and the previous tank temperature (T_t). Heat loss from the tank to the surrounding environment was calculated based on the tank surface area, the tank heat transfer coefficient (U_t), and the temperature difference between water in the tank and the ambient air. In this study, the heat loss was subtracted from the total energy in the tank at each time step to improve the accuracy of temperature predictions. Furthermore, the model simulated the process dynamically with a minute-by-minute resolution, enabling accurate representation of temperature fluctuations from variations in solar radiation and environmental conditions.

•Mixing of the incoming fluid and the fluid in the tank:

$$T_{\text{new}} = (1 - r) \times T_i + r \times T_{\text{out}} \tag{10}$$

where, T_{new} was the average temperature of the fluid in the tank after mixing. T_i signified the fluid temperature in the tank before mixing, and T_{out} was the temperature of the fluid entering the tank.

The parameter r represented the ratio of the incoming fluid mass to the total fluid mass in the tank and was determined as follows:

$$r = \frac{m \times \Delta T}{m_t} \tag{11}$$

where, $\dot{m}$ was the mass flow rate of the incoming fluid (kg/s). The parameter Δt represented the time interval (s), and m_t was the total mass of the fluid in the tank (kg).

•Tank heat loss to the environment:

$$Q_{L,t} = U_t \times A_t \times (T_{new} - T_a) \times \Delta t \tag{12}$$

where, $Q_{L,t}$ was the amount of heat lost from the tank to the environment (Joules), and U_t signified the total heat transfer coefficient from the tank to the air (W m^{-2} K). The variable A_t represented the surface area of the tank interacting with the air (m^2), and T_{new} was the temperature of the fluid in the tank after mixing (℃). Additionally, T_a signified the ambient air temperature (℃), and Δt was the duration of the heat transfer (s).

•Temperature adjustment due to heat loss:

$$T_{new} = T_{new} - \frac{Q_{L,t}}{m_t \times C_p} \tag{13}$$

where, T_{new} signified the fluid temperature after adjusting for heat loss in the Equation, while $Q_{L,t}$ was the amount of heat lost to the environment (Joules). The variable m_t represented the mass of the fluid in the tank (kg), and C_p was the specific heat capacity of the fluid (J kg^{-1} K). This Equation represented the temperature decrease from the loss of heat energy from the fluid over a specified period.

2.4.5 Statistical equation

A statistical equation was used to quantitatively evaluate the performance of the simulation model against experimental data. This method enabled the assessment of both the magnitude of errors and the degree to which the simulation accurately represented the experimental results. The first of the three main primary performance indicators was the root-mean-square error (RMSE), defined as:

$$T_{new} = T_{new} - \frac{Q_{L,t}}{m_t \times C_p} \tag{14}$$

In the context of evaluating simulation results, $T_{sim,i}$ was the simulated temperature at time i, while $T_{exp,i}$ represented the experimentally measured temperature at time i. These values were compared across multiple time points, with the total sum signified by n.

The performance of the simulation model against experimental data was evaluated using three additional statistical metrics, namely MAE, MBE, and R^2. These metrics provided a more comprehensive assessment of the accuracy and bias tendencies of the simulation results.

Mathematically, the formulas for these three metrics were written as follows:

$$MAE = \frac{1}{n} \sum_{i=1}^{n} |T_{\text{sim},i} - T_{\text{exp},i}| \tag{15}$$

$$MBE = \frac{1}{n} \sum_{i=1}^{n} |T_{\text{sim},i} - T_{\text{exp},i}| \tag{16}$$

$$R^2 = 1 - \frac{\sum_{i=1}^{n} \left(T_{exp,i} - T_{\mathrm{sim},i}\right)^2}{\sum_{i=1}^{n} \left(T_{exp,i} - T_{exp}\right)^2} \tag{17}$$

where, $T_{\mathrm{sim},i}$ and $T_{\mathrm{exp},i}$ represented the simulated and experimental temperatures at time i, respectively. The variable n was the total number of data points and T_{exp} signified the average experimental temperature. MAE showed the average absolute difference between the simulated and the experimental values. Consequently, MBE accounted for the direction of the error, showing how the simulation systematically overstimated (positive MBE) or underestimated (negative MBE) the experimental results. R^2 quantified the extent to which the simulation results reproduced the distribution of experimental data. An R^2 value close to 1 showed an excellent fit between simulation and experiment.

2.5 Flowchart of Simulation Procedure

Figure 2 shows the simulation workflow used to model the thermal performance of a lightweight trickle-flow SWH. The process started with input of experimental data and system parameters, followed by preprocessing steps such as data interpolation and assignment. The core of the model was a minute-based simulation loop, which calculated heat loss coefficient, flow factor, and net energy gain at each time step. The tank temperature was then updated based on mixing and losses. After the completion of the simulation loop, the results were validated statistically (e.g., RMSE, MBE) and visualized through temperature trends, efficiency contours, and confidence bands. Parametric studies were subsequently conducted to evaluate the influence of flow rate and tank volume on system performance.

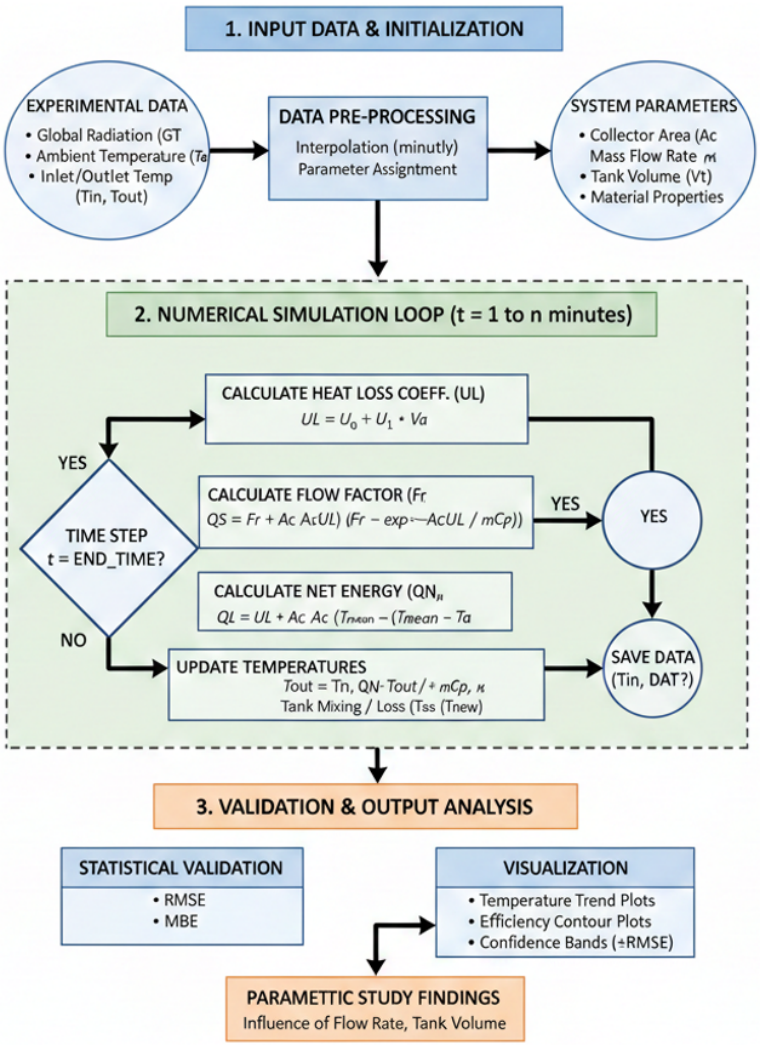

Figure 2. Flowchart of the python-based thermal simulation model for trickle-flow solar water heater, including input parameters, core computations, and statistical validation

3 Results and Discussion

3.1 Comparison of Simulation Results and Experimental Data for Inlet and Outlet Water Temperatures in the SWH Collector

Temperature validation was performed by comparing the simulated the outlet water temperature T_{out} with experimental measurements over the period from 9:00 a.m. to 3:00 p.m., as shown in Figure 3. The simulation predicted a maximum outlet temperature of $T_{\text{out,max}}$ = 45.0℃ at 1:30 p.m, which closely matched the experimental peak of 45.3℃. This strong agreement showed that the numerical model accurately represented the thermal performance of the wave-type solar collector system.

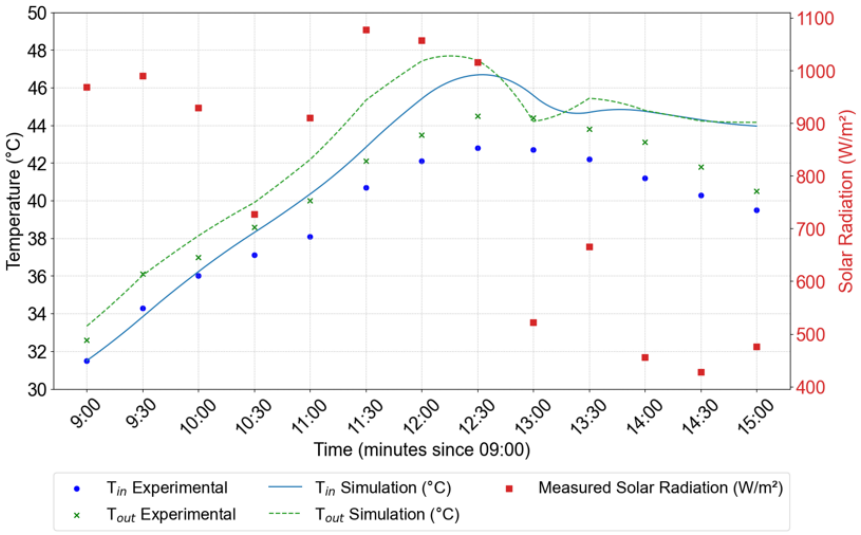

Figure 3. Comparison of simulation results and experimental data for inlet and outlet water temperatures in a SWH collector

The simulation successfully replicated the decreasing temperature trend observed after 2:00 p.m. This showed consistency in the model's predictions of system performance. The accuracy of the model during the process was quantified using RMSE. For the collector orientation due east, the RMSE was 0.9℃. Maeanwhile, the RMSE increased slightly to 1.4℃ for the east +30° orientation.

The low RMSE value showed that the difference between the simulation results and the experimental data were relatively small and acceptable for a household-scale SWH system. Previous studies recommended that an RMSE less than 2℃ represented high accuracy for numerical models of solar collectors. Accordingly, the model developed in this study was considered valid and capable of realistically capturing heat transfer dynamics of the system. These results reinforced the utility of the model as a reliable tool for simulating the performance and guiding the design of the collector systems under varying environmental conditions.

During the analysis, a significant deviation was observed around 12:30 p.m, when the experimental data showed a decrease in temperature despite an increase in G_T. This inconsistency was probably caused by a delay in the temperature sensor response or an error in the measurement of G_T during the experiment. In general, the simulation model successfully provided realistic temperature predictions and could be used as a tool for the design and optimization of the SWH system.

3.2 Effect of Flow Rate on T_{in}, T_{out} and ΔT

The fluid flow rate played a crucial role in determining the performance of a solar collector system. Figure 4 shows how variations in flow rate (in LPM) affected three major parameters. The variables included collector inlet temperature (T_{in}), collector outlet temperature (T_{out}), and temperature difference ($\Delta T = T_{\text{out}} - T_{\text{in}}$). At a low flow rate, the fluid remained in the collector for a longer period, causing a significant increase in ΔT. At a high flow rate, ΔT decreased because the shorter residence time reduced the amount of heat absorbed per unit mass. However, increasing the flow rate led to a high T_{in}, as rapid circulation maintained the overall tank temperature. Understanding this relationship was crucial for the design of an efficient SWH system.

The graph explains the trade-off between the temperature increase per liter of water (ΔT) and the total heating capacity of the system. At low flow rates, the water temperature rise is high, but the total stored energy is limited due to the small volume of water circulated. At high flow rates, more total energy is stored, although each liter of water experiences a smaller temperature increase. The analysis helps identify the optimal operating point, depending

on how the system prioritizes water temperature (quality) or total energy storage (quantity). These perceptions are crucial for practical applications, such as selecting an appropriate circulation pump and designing a suitably sized tank for household or small-scale industrial SWH systems.

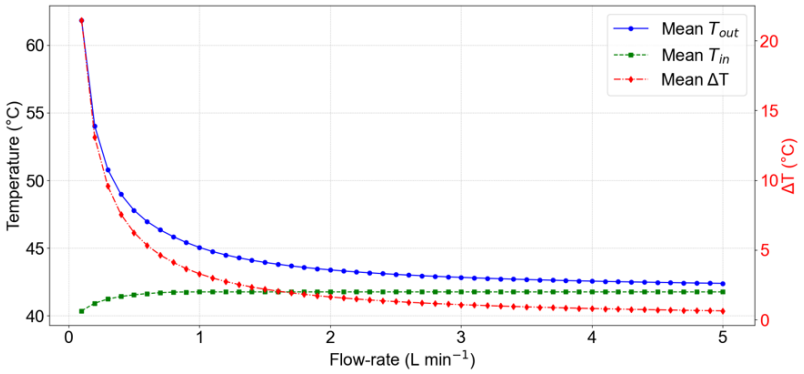

Figure 4. Effect of flow rate on T_{in}, T_{out} and ΔT

3.3 Analysis of Collector Efficiency Contour Based on Flow Rate and Tank Volume

Figure 5 shows a contour graph signifying the relationship between fluid flow rate and tank volume on the efficiency of the solar collector. The curved contour pattern indicated that an optimal combination of these two variables existed to achieve maximum efficiency. At very low flow rates, collector efficiency decreased due to overheating and excessive heat accumulation. Meanwhile, at higher flow rates, efficiency decreased because of reduced fluid residence time. Tank volume also influenced temperature stability, as a smaller tank could not store energy optimally, and a larger tank might experience greater heat losses.

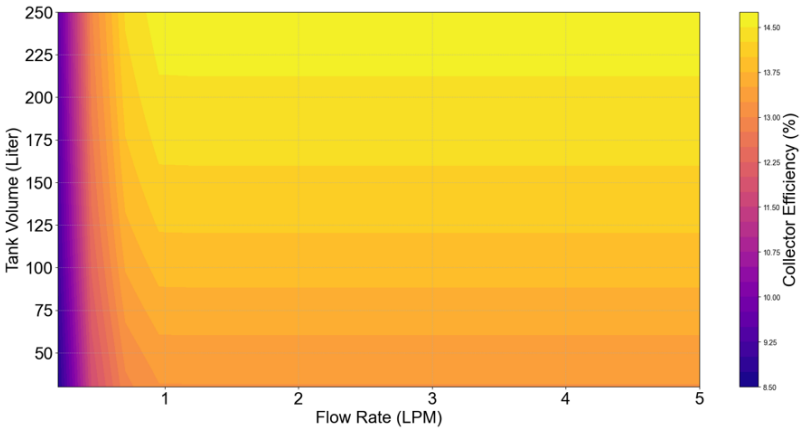

Figure 5. Collector efficiency contour based on flow rate and tank volume

The contour chart provides a valuable visual tool for the design of future SWH systems. By identifying the optimal zone for the combination of flow rate and tank volume, designers can develop systems that balance size, efficiency, and production cost. This information is particularly useful for creating compact SWH systems that achieve maximum performance suitable for residential applications or remote areas with limited space and budget. Furthermore, the chart aids designers in selecting system configurations that are well-adapted to local climate conditions.

3.4 Model Accuracy Evaluation with RMSE and Confidence Band

The RMSE metric is used to assess how accurately the numerical model represents experimental conditions. RMSE is widely used in numerical modeling because it quantifies the average magnitude of error between the simulation results and the observed data. A smaller RMSE value indicates that the model predictions closely approximate the actual system behavior.

In this study, RMSE was used to assess the accuracy of the model for the collector T_{in} (Figure 6) and T_{out} (Figure 7). The calculation yielded an RMSE of 2.78℃ for T_{in} and 2.28℃ for T_{out}. These results signified that the

average difference between the simulation and experimental temperature was relatively small and remained in the acceptable tolerance limits for SWH systems.

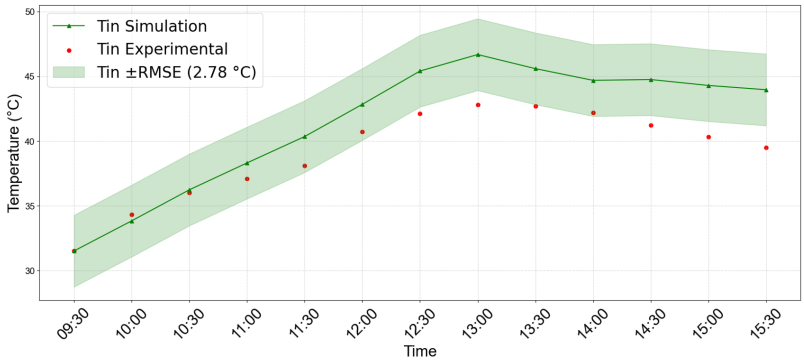

Figure 6. Graph of collector inlet temperature (T_{in}) from simulation results and experimental data with confidence bands ± RMSE

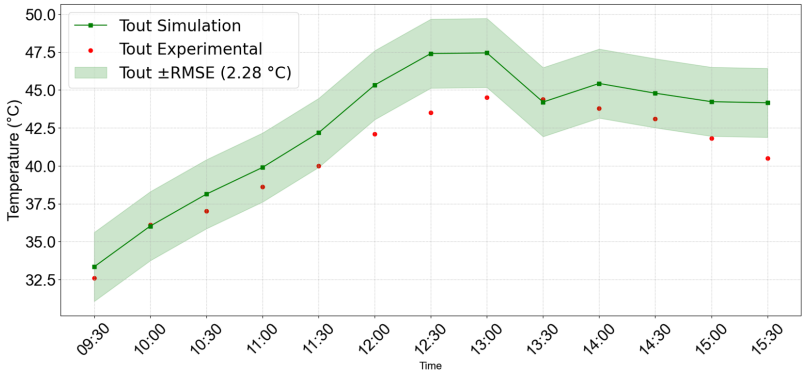

Figure 7. Graph of collector outlet temperature (T_{out}) from simulation results and experimental data with confidence bands ± RMSE

A confidence band method was used to visually represent the error of the model, with ± RMSE limits plotted around the simulation curve. These bands represented the range in which the experimental measurements were expected to fall when the model performed consistently. Since the RMSE formula formed the basis for constructing these confidence bands, the discussion of the two variables was combined.

The visualization in Figure 6 (T_{in}) and Figure 7 (T_{out}) show that most of the experimental data fall in the ± RMSE confidence band. The simulation curves closely follow the experimental trend, indicating the reliability of the numerical model in predicting the thermal behavior of the wave-type solar collector system.

3.5 Evaluation with Statistical Metrics MAE, MBE, and Coefficient of Determination (R^2)

The performance of the simulation model against experimental data was further evaluated using MAE, MBE, and R^2. These metrics provided a more comprehensive assessment of the accuracy and bias tendencies of the simulation results.

MAE measured the average absolute error between the simulation results and the experimental data, irrespective of the direction of the error. A low MAE value showed a good predictive performance of the model. On the other hand, MBE provided information on the systematic tendency of the model to overestimate (positive) or underestimate (negative). R^2 measured the proportion of variability in the experimental data explained by the model, with values close to 1 indicating an excellent fit.

Figure 8 shows the evaluation results of MAE, MBE, and R^2 for both T_{in} and T_{out}. For the T_{in}, MAE and MBE were both 2.91℃, while R^2 was 0.934. For T_{out}, MAE and MBE were 2.47℃ MBE with an R^2 of 0.957. These results indicated that the model showed relatively low MAE and MBE values. The high R^2 values signified that the simulation accurately captured the experimental temperature trends.

Based on the statistical evaluation results, the following discussion examined the consistency and reliability of the model in representing system performance under various operating conditions. This ensured that the observed agreement was not limited to a single experimental configuration. Although the experimental validation in this

study was conducted using one test setup, the correspondence between the numerical model and the measured data was supported by consistent trends observed in the parametric analysis. Variations in mass flow rate and storage tank volume produced systematic and predictable changes in outlet water temperature and overall system efficiency [15, 22]. An increase in mass flow rate generally decreased the outlet temperature and improved system efficiency. Meanwhile, a larger storage tank volume improved temperature stability and thermal performance [23, 24]. These responses were consistent with the well-established behavior of solar thermal systems. The process indicated that the agreement between the model experimental results was not incidental to specific test conditions.

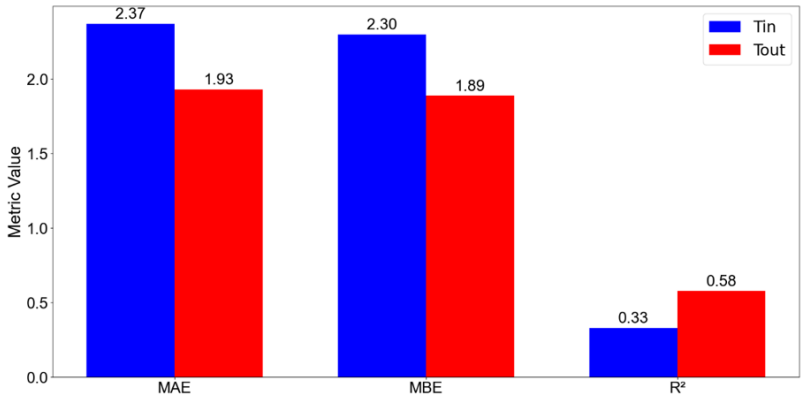

Figure 8. Bar chart comparing the statistical metrics MAE, MBE, and R^2 between the simulation and experimental results for the inlet temperature (T_{in}) and outlet temperature (T_{out})

4 Conclusion

In conclusion, this study developed and validated a transient numerical model for a lightweight trickle-flow SHW system, with the implementation conducted in Python. The model was designed to reproduce the dynamic behavior of fluid inlet and outlet temperatures based on experimental measurements as well as microclimate variables.

The simulation results showed that the fluid temperature trends predicted by the model were in good agreement with the experimental data, particularly for the east-oriented collector, with a maximum temperature deviation of approximately 0.3℃. The RMSE values were 2.78℃ for T_{in} and 2.28℃ for T_{out}. Meanwhile, the corresponding MAE values were 2.91℃ and 2.47℃. R^2 reached 0.934 for T_{in} and 0.957 T_{out}, indicating a high level of accuracy in predicting the thermal performance of the system. In addition, the visualization using confidence bands further confirmed that most experimental data points were in the ± RMSE range of the simulation results.

The model was applied to evaluate the influence of fluid flow rate on $T_{\text{in}}, T_{\text{out}}$, and ΔT beyond numerical validation. The results showed that at low flow rates, the fluid remained in the collector for a longer residence time, leading to an increase in ΔT. On the other hand, the total amount of thermal energy stored was relatively limited. Higher flow rates produced a lower ΔT and increased the volume of heated fluid, leading to greater overall energy collection. This behavior showed a fundamental trade-off between heating quality and quantity.

The simulations signified that collector efficiency was strongly influenced by the interaction between fluid flow rate and storage tank volume. The efficiency contours analysis showed the existence of an optimal operating region in which a balance between flow rate and tank volume maximized collector performance. Following the discussion, an excessively low flow rate led to overheating and heat accumulation in the collector. Meanwhile, an excessively high flow rate reduced the fluid residence time, decreasing the amount of heat absorbed and lowering overall efficiency.

The model successfully validated the experimental results and provided reliable observations for the design and optimization of lightweight SWH systems. This method would be crucial for the development of efficient, economical, and suitable SWH systems for tropical regions such as Indonesia.

Further evaluation is required to ensure that the predictive capability of the SWH system can be maintained under a wider range of operating conditions, even though the results obtained show promising model performance. Therefore, the current validation should be considered an initial verification of the proposed lumped-parameter model. Future studies should focus on extending the experimental validation by incorporating variations in operating conditions. In addition, the studies should also focus on different collector orientations and longer measurement periods to more comprehensively assess the generalizability as well as the robustness of the model.

Author Contributions

Conceptualization, N.A.P.; methodology, N.A.P.; validation, N.A.P.; formal analysis, D.M.M.S. and D.R.S.P.P.; investigation, D.M.M.S. and D.R.S.P.P.; resources, N.A.P.; data curation, D.M.M.S., D.R.S.P.P., and D.K.U.;

writing—original draft preparation, D.M.M.S. and D.R.S.P.P.; writing—review and editing, N.A.P. and D.K.U.; visualization, D.M.M.S. and D.R.S.P.P.; supervision, N.A.P.; project administration, N.A.P. and D.K.U. All authors were actively involved in discussing the findings and refining the final manuscript.

Data Availability

The data used to support the findings of this study are available from the corresponding author upon request.

Acknowledgments

The authors are grateful to the Directorate of Research and Community Service (DPPM) with Grant Number 105/C3/DT.05.00/PL/2025 and 1186.1/UN27.22/PT.01.03/2025. The authors are also grateful to the Fundamental Research (PF-DPPM), the Institute for Research and Community Service (LPPM) of Sebelas Maret University, as well as the Ministry of Higher Education, Science, and Technology.

Conflicts of Interest

The authors declare that they have no conflicts of interest.

References

[1] B. K. Sahu, "A study on global solar PV energy developments and policies with special focus on the top ten solar PV power producing countries," *Renew. Sustain. Energy Rev.*, vol. 43, pp. 621–634, 2015. https://doi.org/10.1016/j.rser.2014.11.058

[2] T. Ahmad and D. Zhang, "A critical review of comparative global historical energy consumption and future demand: The story told so far," *Energy Rep.*, vol. 6, pp. 1973–1991, 2020. https://doi.org/10.1016/j.egyr.2020.07.020

[3] S. A. Sulaiman, "Overview of geography, socio-economy, energy and environment of the tropical countries," in *Green Energy and Technology*. Springer Nature, 2021, pp. 1–31.

[4] K. K. P. Kumar, S. R. Atchuta, M. S. Prasad, H. C. Barshilia, and S. Sakthivel, "Review on selective absorber coatings: A catalyst for enhanced solar energy conversion efficiency," *Sol. Energy Mater. Sol. Cells*, vol. 277, p. 113080, 2024. https://doi.org/10.1016/j.solmat.2024.113080

[5] S. E. Hosseini, "Transition away from fossil fuels toward renewables: Lessons from Russia-Ukraine crisis," *Future Energy*, vol. 1, no. 1, pp. 2–5, 2022. https://doi.org/10.55670/fpll.fuen.1.1.8

[6] T. A. Rizal, M. Amin, S. B. Widodo, N. A. Rachman, F. Amir, N. Pane, and T. M. I. Mahlia, "Integration of phase change material in the design of solar concentrator-based water heating system," *Entropy*, vol. 24, no. 1, p. 57, 2021. https://doi.org/10.3390/e24010057

[7] R. A. Kristian, A. G. Safitra, and R. A. Nurisma, "Studi eksperimental pengaruh perubahan debit aliran pada efisiensi termal solar water heater dengan penambahan finned tube," *Pros. Sains Nas. Teknol.*, vol. 1, no. 1, pp. 52–57, 2017.

[8] I. N. Unar, G. Maitlo, S. Ahmed, S. S. Ali, A. Q. Memon, G. A. Kandhro, and A. S. Jatoi, "Performance evaluation of solar flat plate collector using different working fluids through computational fluid dynamics," *SN Appl. Sci.*, vol. 2, no. 2, p. 209, 2020. https://doi.org/10.1007/s42452-020-2005-z

[9] R. R. Rakasiwi, S. Syaifurrahman, and U. A. Gani, "Rancang bangun pemanas air surya tipe datar," *ELKHA*, vol. 10, no. 2, p. 78, 2018. https://doi.org/10.26418/elkha.v10i2.27901

[10] S. E. Frid, A. V. Arsatov, and M. Y. Oshchepkov, "Engineering solutions for polymer composites solar water heaters production," *Therm. Eng.*, vol. 63, no. 6, pp. 399–403, 2016. https://doi.org/10.1134/S0040601516060021

[11] A. Aboulmagd, "Core and accessory polymeric materials for solar water heaters," *Encycl. Mater. Plast. Polym.*, vol. 3, pp. 178–192, 2022. https://doi.org/10.1016/B978-0-12-820352-1.00266-2

[12] S. K. Thangavelu, R. J. Khoo, and C. Piraiarasi, "Exergy and exergoeconomic analysis of domestic scale solar water heater by the effect of solar collector area," *Mater. Today Proc.*, vol. 47, pp. 5004–5010, 2021. https://doi.org/10.1016/j.matpr.2021.04.584

[13] N. I. S. Azha, H. Hussin, M. S. Nasif, and T. Hussain, "Thermal performance enhancement in flat plate solar collector solar water heater: A review," *Processes*, vol. 8, no. 7, p. 756, 2020. https://doi.org/10.3390/pr8070756

[14] D. Harun, M. I. Maulana, T. Syahrul, and M. Ibrahim, "Pengaruh variasi bentuk plat terhadap performansi solar water heater," *J. Tek. Mesin*, vol. 8, no. 1, pp. 7–12, 2020.

[15] A. Remlaoui, D. Nehari, B. Kada, N. A. A. M. Nasir, A. Abd-Elmonem, N. Alhubieshi, F. A. A. ElSeabee, and S. M. Hussain, "Numerical simulation of a forced circulation solar water heating system," *Sci. Rep.*, vol. 14, p. 28999, 2024. https://doi.org/10.1038/s41598-024-80576-y

[16] N. Kaloyanov, R. Tsecov, and N. Penkova, "Modelling and numerical simulation of the transport phenomena in water thermal energy storage tanks," *E3S Web Conf.*, vol. 327, p. 01011, 2021. https://doi.org/10.1051/e3sconf/202132701011

[17] B. Schlagbauer, "Optimization of a solar air heater," Master's thesis, Friedrich-Alexander-Universität Erlangen-Nürnberg, Germany, 2022.

[18] M. Grahovac, K. Coughlin, H. Gerhart, and R. Hosbach, "Scalable solar water heating: Engineering system models," 2025. https://escholarship.org/uc/item/5zh0x7db

[19] D. P. Hiris, O. G. Pop, and M. C. Balan, "Analytical modeling and validation of the thermal behavior of seasonal storage tanks for solar district heating," *Energy Rep.*, vol. 8, pp. 741–755, 2022. https://doi.org/10.1016/j.egyr.2022.07.113

[20] A. R. Khanghahi, M. Zamen, M. Soufari, M. Amidpour, and A. A. Nejad, "Theoretical investigation of consumption patterns effect on optimal orientation of collector in solar water heating system," *J. Renew. Energy Environ.*, vol. 4, no. 1, pp. 1–10, 2017. https://doi.org/10.30501/jree.2017.70101

[21] B. Yunianto, "Uji prestasi pemanas air tenaga matahari jenis tabung dengan variasi arah kolektor terhadap datangnya sinar matahari," *ROTASI*, vol. 22, no. 2, pp. 142–148, 2020. https://doi.org/10.14710/rotasi.22.2.142-148

[22] O. P. Sunkarwar, B. K. Naik, and A. Dasore, "Experimental and numerical study of parallel flow evacuated u-tube solar collector with parabolic reflector: Impact of particulate matterr," *J. Sol. Energy Eng.*, vol. 147, no. 4, p. 041001, 2025. https://doi.org/10.1115/1.4067664

[23] N. A. Pambudi, Y. Ahnaf, I. R. Nanda, M. Aziz, D. K. Ulfa, and H. A. Rahayu, "Analysis of serpentine collector performance based on flow rate variation for improving efficiency and environmental impact of solar water heater," *J. Sustain. Dev. Energy Water Environ. Syst.*, vol. 13, no. 1, pp. 1–15, 2025. https://doi.org/10.13044/j.sdewes.d13.0547

[24] W. K. Jabbar, A. K. Alshara, and A. S. Allawy, "Numerical analysis of a solar thermal energy storage tank filled with phase change material under three fin arrangements," *Int. J. Thermofluids*, vol. 24, p. 100965, 2024. https://doi.org/10.1016/j.ijft.2024.100965

Nomenclature

G_T	Global solar radiation intensity, W/m^2
V_a	Wind speed at the collector surface, m/s
T_{out}	Outlet water temperature, ℃
U_0	Convective heat loss coefficient, W/m^2·K
η_0	Ideal collector efficiency
T_f	Fluid temperature in the collector, ℃
α	Absorptance of the absorber plate
Q_S	Heat absorbed by the collector, W
Q_L	Heat loss from the collector, W
Q_N	Net heat to water, W
$\dot{m}$	Mass flow rate, kg/s
η_f	Collector flow factor
T_t	Tank fluid temperature, ℃
T_a	Ambient air temperature, ℃
$Q_{L,t}$	Heat loss from the tank, J
A_t	Tank surface area, m^2
RMSE	Root Mean Square Error, ℃
MBE	Mean Bias Error
T_{in}	Inlet water temperature, ℃
U_L	Total heat loss coefficient
U_1	Forced convective heat loss coefficient, W/m^2·K
η_c	Actual collector efficiency
τ	Transmittance of transparent cover
$G_{T,\text{eff}}$	Effective radiation absorbed, W/m^2
A_c	Collector surface area, m^2
T_m	Mean fluid temperature in the collector, ℃
ΔT	Temperature rise, ℃

C_p	Specific heat capacity of water, J/kg·K
e	Euler's number (≈ 2.718)
T_i	Fluid temperature before mixing, ℃
m_t	Total mass of water in the tank, kg
U_t	Heat transfer coefficient for tank, W/m^2·K
Δt	Time interval, s
MAE	Mean Absolute Error, ℃
R^2	Coefficient of determination